

# Evaluating the Maximum Likelihood Method for Detecting Short-Term Variability of AGILE $\gamma$ -ray Sources

A. Bulgarelli<sup>1</sup>, A.W. Chen<sup>3</sup>, M. Tavani<sup>2,4</sup>, F. Gianotti<sup>1</sup>, M. Trifoglio<sup>1</sup>, T. Contessi<sup>3</sup>

<sup>1</sup>INAF/IASF–Bologna, Via Gobetti 101, I-40129 Bologna, Italy

<sup>2</sup>INAF/IASF–Roma, Via del Fosso del Cavaliere 100, I-00133 Roma, Italy

<sup>3</sup>INAF/IASF–Milano, Via E. Bassini 15, I-20133 Milano, Italy

<sup>4</sup>Dip. di Fisica, Univ. “Tor Vergata”, Via della Ricerca Scientifica 1, I-00133 Roma, Italy

received; accepted

## ABSTRACT

**Context.** The AGILE space mission (whose instrument is sensitive in the energy ranges 18-60 keV, and 30 MeV - 50 GeV) has been operating since 2007. Assessing the statistical significance of time variability of  $\gamma$ -ray sources above 100 MeV is a primary task of the AGILE data analysis. In particular, it is important to check the instrument sensitivity in terms of Poisson modeling of the data background, and to determine the post-trial confidence of detections.

**Aims.** The goals of this work are: (i) evaluating the distributions of the likelihood ratio test for “empty” fields, and for regions of the Galactic plane; (ii) calculating the probability of false detection over multiple time intervals.

**Methods.** In this paper we describe in detail the techniques used to search for short-term variability in the AGILE  $\gamma$ -ray source database. We describe the binned maximum likelihood method used for the analysis of AGILE data, and the numerical simulations that support the characterization of the statistical analysis. We apply our method to both Galactic and extra-galactic transients, and provide a few examples.

**Results.** After having checked the reliability of the statistical description tested with the real AGILE data, we obtain the distribution of  $p$ -values for blind and specific source searches. We apply our results to the determination of the post-trial statistical significance of detections of transient  $\gamma$ -ray sources in terms of pre-trial values.

**Conclusions.** The results of our analysis allow a precise determination of the post-trial significance of  $\gamma$ -ray sources detected by AGILE.

**Key words.**  $\gamma$ -rays: general; Methods: statistical; Methods: data analysis;

## 1. Introduction

The current generation of  $\gamma$ -ray space missions, AGILE and Fermi, are sensitive in the energy range above 100 MeV up to tens of hundreds of GeV. These missions are providing a great wealth of data on a variety of  $\gamma$ -ray sources, both in our Galaxy and at extragalactic distances. Compared with the previous generation of  $\gamma$ -ray instruments (e.g., EGRET on board of the Compton Gamma-Ray Observatory), the AGILE and Fermi-LAT  $\gamma$ -ray imagers are based on silicon detectors with optimal spatial resolution and much improved background rejection. These characteristics allow reaching a few arcminute positioning for intense sources and very large fields of view (FOVs). Both AGILE and Fermi-LAT reach FOVs more than 100 degrees across, i.e., 2.5 sr, and this fact is of great relevance for the statistical analysis of the  $\gamma$ -ray sources. Based on the current detector performances, it is crucial to perform a statistical analysis specialized to the specific modes of operation of the two  $\gamma$ -ray missions. In particular, the distinction between non-significant and significant steady/transient sources must be supported by a specific treatment of the satellite  $\gamma$ -ray data. The relatively large effective areas at  $\gamma$ -ray energies, and the very large FOVs, produce large exposures (measured as the product of effective area times the on-source duration). The statistical significance of  $\gamma$ -

ray source detections must address the pre- vs. post-trial significance. As we will see, the characteristics of the pointing and of the specific search (whether a “blind” search or a search for a specific source) have a direct influence on the proper statistical treatment. In this paper, we address the issue of the statistical determination of  $\gamma$ -ray sources for the AGILE mission.

The AGILE-GRID instrument for observations in the  $\gamma$ -ray has an energy range of 30 MeV - 50 GeV (Tavani et al. 2009a). AGILE data are down-linked approximately every 100 minutes and sent to the AGILE Data Center (ADC), which is part of the ASI Science Data Center (ASDC) for data reduction, scientific processing, and archiving. ASDC forwards the AGILE data to the AGILE Team local sites where a Quick Look analysis is performed.

Because of the low detection rate of events and the extent of the AGILE GRID point-spread function (PSF), statistical techniques like the maximum likelihood method (or estimator) are required to analyze the AGILE point sources. Similar analysis techniques were used for EGRET data (Mattox et al. 1996).

For steady sources and sources with high  $\gamma$ -ray flux, the significance of a detection increases as a function of the observation duration. This is not necessarily the case for variable sources with low flux: a short integration time (the integration period should be of the same time scale as the duration of the astronomical phenomena under study) may yield a low significance level because the observation is *photon limited*; for a longer in-

Send offprint requests to: A. Bulgarelli, e-mail: bulgarelli@iasfbo.inaf.it

tegration time the source may disappear entirely because the observation is *background limited*.

The main purpose of this work is the evaluation of the likelihood ratio test in the context of short time scale (1-2 days) flaring  $\gamma$ -ray sources. The likelihood ratio test is used to compare two ensembles of hypotheses, one in which a  $\gamma$ -ray source is present, and another (the null hypothesis) in which it is absent. The determination of the likelihood ratio distribution in the case of the null hypothesis is used to evaluate the occurrence of false positive detections.

The search for  $\gamma$ -ray transients (Galactic and extra-Galactic) detectable on timescales of 1-2 days is one of the major activities performed by the AGILE Collaboration<sup>1</sup>.

The main goals of this work are: (i) to evaluate the distribution of the likelihood ratio test statistic ( $T_s$ ) for empty fields both outside of and within the Galactic plane; (ii) to evaluate the  $T_s$  distribution in the case of one flaring source with different combinations of parameters; and (iii) to calculate the confidence levels corresponding to the same false detection probability in multiple non-overlapping time periods.

We performed Monte Carlo simulations to determine the  $T_s$  distributions both in the presence and absence of a flaring source, which may differ from the theoretically predicted distribution for a number of reasons which we discuss below. We compare these results with the AGILE data where feasible, and show *how the formulation of the hypotheses influences the  $T_s$  distribution*.

In Section 2 we present the AGILE -GRID maximum likelihood analysis method. In Section 3 we report a general description of the performed Monte Carlo simulations. In Section 4 we characterize the  $T_s$  distribution of a simulated extra-Galactic empty field and compare it with a real observation case. Section 5 characterizes the  $T_s$  distribution for two simulated Galactic fields, a simple and a complex case; in the latter we analyze the effect that uncertainties in the analysis parameters produce on the  $T_s$  distribution. In Section 6 we describe the pre- and post-trial probability, and in Section 7 we consider multiple detections from the same sky position.

## 2. Analysis method

The **likelihood ratio test** is used to compare two ensembles of models, one of which is a subset of the other, each of which can be characterized by a set of parameters. In the most common case, one of the ensembles of models is the null hypothesis, while the other, of which the null hypothesis is a subset, is the alternative hypothesis, corresponding to, for example, the hypothesis of the existence of a source. In each case, the values of the set of parameters are found by means of a maximum likelihood method or estimator which maximizes the **likelihood** of producing the data given the ensemble of models. The application of likelihood to photon-counting experiments is described in (Cash 1979). Details of how the likelihood is calculated in the context of  $\gamma$ -ray data analysis can be found in (Mattox et al. 1996). The likelihood ratio is then simply the ra-

tio of these two maximum likelihoods, and the test statistic  $T_s$  is defined as

$$T_s = -2 \ln \frac{L_0}{L_1} \quad (1)$$

where  $L_0$  and  $L_1$  are the maximum value of the likelihood function for the null hypothesis and for the alternative hypothesis, respectively.

In the AGILE-GRID case, the data are binned into FITS counts maps, while each model is a linear combination of isotropic and Galactic diffuse components of the  $\gamma$ -ray emission and point sources.  $\gamma$ -ray exposure maps, and galactic diffuse emission maps are used to calculate the models. Among the parameters which may be varied to find the maximum likelihood are the coefficients of the diffuse and point source components.

In general, to describe a single point source, four parameters are used: the predicted source counts  $s_c$ , the spectral index  $s_{si}$  (the spectrum of each source is assumed to be a power-law), and two parameters corresponding to the position of the source ( $s_l, s_b$ , in Galactic coordinates). It is possible to keep each parameter free or fixed; a free parameter is allowed to vary to find the maximum likelihood. Possible combinations include: only allowing the flux to vary, allowing both the position and flux to vary, allowing both the spectrum and flux to vary, or leaving all four parameters free. Throughout this paper we keep the spectral index fixed to 2.1; for this kind of sources the AGILE-GRID instrument has a point spread functions (PSF) at 30° off-axis for E>100 MeV of 2.1°, for E>400 MeV of 1.1°, for E>1 GeV of 0.8°.

The two parameters that describe the Galactic (diffuse) and isotropic  $\gamma$ -ray emission are: (i)  $g_{gal}$ , the coefficient of the Galactic diffuse emission model, and (ii)  $g_{iso}$ , the isotropic diffuse intensity. A value of  $g_{gal} \leq 1$  is expected if the galactic diffuse emission model is correct. Values of  $g_{iso}$  between 1 and  $15 \times 10^{-5} \text{cm}^{-2} \text{s}^{-1} \text{sr}^{-1}$  are expected, depending on pointing strategy and on board and background filter rejection. These two parameters can be left free or fixed independently. For short timescale variability (less than 3-4 days) of  $\gamma$ -ray sources, usually we first estimate these parameters with a longer timescale integration, and then fix them for the short timescale analysis, assuming that these components do not vary significantly on the shorter timescales. We note that for the AGILE data used in this analysis (based on the standard filter FM3.119), the isotropic component is dominated by instrumental charged particle background rather than by the extragalactic diffuse emission, in contrast to data from EGRET and Fermi-LAT.

The values of the parameters which maximize the likelihood are those which describe the model in the ensemble most likely to reproduce the data.

The null hypothesis corresponds to the absence of the point source, while the alternative hypothesis corresponds to its presence. Clearly, the null hypothesis is a subset of the alternative hypothesis, corresponding to a source with zero flux. The Galactic diffuse and isotropic coefficients, as well as the parameters of other known point sources in the field of view, must be kept either fixed or free in the same manner when evaluating both the null and alternative hypothesis.

In order to limit the effect of systematic errors far from the position of the hypothesized source, the data bins evaluated (and their predicted values according to the models) are limited to an **analysis region** of radius 5° or 10° centered around the source position.

From Wilks's Theorem (Wilks 1938) the  $T_s$  distribution  $\varphi$  is expected to asymptotically follow  $\chi^2_{n-m}$  in the null hypothesis,

<sup>1</sup> Two independent  $\gamma$ -ray transient search systems have been developed. One system operates at INAF/IASF-Bologna (Bulgarelli et al. 2009); it is able to process the data within 1.5 hours (from the last photon acquired in orbit to the alert generation), and to generate alerts via e-mail and SMS to the mobile phones of the AGILE Collaboration. A second system operates at the ADC (AGILE Data Center) in Frascati; it can react within an average time of 3 hours, and generates alerts via e-mail but with more accurate data processing.

where  $n - m$  is the number of additional parameters that are optimized in the alternative hypothesis. In the most simple case,  $n - m = 1$  (e.g., in the case of the determination of the flux of a single source). This means that from Wilks's theorem,  $T_s$  is expected to be asymptotically distributed as  $\chi_1^2$  in the null hypothesis. The expected departure of the distribution from  $\chi_1^2$  is of order  $(N)^{-1/2}$  where  $N$  is the number of **samples**. In our context, the number of samples is the number of photons which carry information about all the parameters; these are all the photons in the analysis region. This is true regardless of the number that is eventually estimated to come from the point source.

When there are multiple sources whose fluxes are allowed to vary, the following procedure, divided into two loops, is used to find the maximum  $T_s$ . In the first loop, first the sources are sorted according to hypothesized flux. One by one, the sources are added to the model, from highest to lowest flux. If the source flux is allowed to vary, then the maximum likelihood is found both in the presence and absence of the source. If the position is allowed to vary, the first fit is done at a fixed position and the resulting  $T_s$  is compared to a location confidence level threshold ( $t_{lcl}$ ). If  $T_s > t_{lcl}$ , then  $T_s$  is again maximized with variable flux and position.  $T_{ss}$  is a threshold for promoting the source to the second loop of the algorithm: if the final  $T_s$  is greater than  $T_{ss}$ , the source is considered significant and added to both the null and alternative hypotheses for the other sources. If not, it is considered undetected, and is set to zero flux for all subsequent analyses. With the sources over the  $T_{ss}$  threshold (with or without a location confidence level) the second loop is similar to the first loop, except that all of the sources marked significant in the first loop are contained in the models from the beginning. The sources are again evaluated one at a time from highest to lowest flux. The  $T_s$  of each source is again maximized, and set to its final value. The values of the parameters  $t_{lcl}$  and  $T_{ss}$  affect the behavior of the procedure.  $t_{lcl} = 5.99147$  corresponds to a 95% confidence level for two degrees of freedom.

The maximum likelihood estimator developed for AGILE constrains the flux of a source, and therefore the source counts  $s_c$ , to be greater than or equal to zero. Because the ensemble of models considered is half of the theoretically possible number, the shape of the  $T_s$  distribution differs from that of Wilks's theorem by being asymptotically distributed as  $0.5 \times \chi_1^2$  instead of  $\chi_1^2$  (Mattox et al. 1996).

In order to compare the data distribution of  $T_s$  produced by the AGILE analysis procedure with that predicted by Wilks's theorem, we performed a series of Monte Carlo simulations of AGILE data. Each simulation of an analysis region and its subsequent maximum likelihood analysis constitutes a single trial. The probability that the result of a trial in an empty field has  $T_s \geq h$  (that is the complement of the cumulative distribution function) is

$$P(T_s \geq h) = \int_h^{+\infty} \varphi(x) dx \quad (2)$$

This is also called the  $p$ -value  $p = P(T_s \geq h)$ . This is the pre-set (pre-trial) type-1 error (a false positive, rejecting the null hypothesis when in fact it is true). Given a statistical distribution, a " $p$ -value" assigned to a given value of a random variable is defined as the probability of obtaining that value or larger when the null hypothesis is true. This value may be interpreted as an "occurrence-rate", that is, how many trials occur on average before obtaining a false detection at a level equal or greater to  $h$ .

## 2.1. Hypothesis formulation

In the context of the  $\gamma$ -ray transient analysis, the null hypothesis is defined as an analysis region containing only steady and known sources with no flaring sources present. We can translate this into the ensemble of models by keeping the flux of the flaring source fixed to zero, and the fluxes of steady sources fixed to their known fluxes. In the alternative hypothesis that a flaring source is present, the flux (and position if specified) of this source is allowed to be free and the fluxes of steady sources are fixed to their known fluxes. In this work, we restrict our analysis to hypotheses of single flaring sources, neglecting alternative hypotheses of 2 or more flaring sources in the same analysis region.

Additional knowledge of the source, e.g. from other wavelengths, can add useful additional constraints about the position of the source in the hypothesis formulation. In Section 5 we show that this additional knowledge can change the  $T_s$  distribution, and thereby reduce the occurrence rate of false detection.

For the analysis of a flaring source, we consider two possible scenarios:

1. The flaring source is unknown: in this case, the position and flux parameters are allowed to be free and optimized with respect to the input data: the starting ( $l, b$ ) position is usually the counts peak found in the smoothed map. If the  $T_s$  is higher than a well defined threshold, the alternative (flaring source) hypothesis is accepted, and a counterpart search may be performed.
2. The source is known and the alternative hypothesis is that this source is in flaring state. This scenario can be further subdivided into two cases:
  - (a) The mean flux of the source is below the background level of the sky region, producing only an upper limit over long integrations.
  - (b) The mean flux of the source is above the background level of the sky region and is detected over long integrations.

In both sub-cases, two types of analysis are possible: (i) the flux parameter is allowed to be free and the position kept fixed, (ii) the flux and position parameters are allowed to be free. If the position is allowed to be free, the starting position is usually the position of the source in steady state. Keeping the position fixed implies that the alternative hypothesis being tested is that the flare comes from the known source (e.g. from the behaviour in other wavelengths or because other flares have been detected in the past), whereas allowing the position to vary allows the alternative hypothesis to include any flaring source within the analysis region. We may then, at the same time as we calculate the significance of the detection, verify whether the confidence contour of the source position is compatible with the source hypothesized to be responsible for the flare. If the position of the known source is outside the confidence region then the alternative hypothesis can be rejected in the sense that the known source is not responsible for the flare.

## 3. Monte Carlo simulations

Monte Carlo simulations of AGILE  $\gamma$ -ray data were used to characterize the maximum likelihood analysis procedure. Simulated data were generated using a model of the background (Galactic diffuse radiation model and isotropic background) and the AGILE-GRID instrument response functions (version I0023

of the calibration matrices for effective area, energy dispersion and point spread function). The energy range used is 100 MeV - 50 GeV. The simulated observations were generated adding Poisson-distributed deviates to each pixel. Each bin of the generated maps (counts, exposure and Galactic emission maps) has been analyzed exactly as flight data as described in Section 2. The bin size chosen for the simulations is  $0.25^\circ$ , the same size used in the AGILE-GRID daily monitoring.

The exposure level chosen for the simulations was a level equivalent to a mean value of 1-day pointing/2-day spinning AGILE observation mode.

In Table 1 we report the parameters and the number of trials for the performed simulations.

## 4. Extra-Galactic empty field

### 4.1. Monte Carlo simulation

We simulated an extra-Galactic empty field without flaring or steady sources. The simulation was performed with an AGILE field of view of  $60^\circ$ . Figure 1 shows the exposure map, and the bins used in this simulation to perform the trials. This is a typical 2-day exposure map in spinning mode, but in this context the key point is the level of exposure, and not its shape. We analyzed positions within  $50^\circ$  of the center of the map to exclude low values of the exposure, which we also do in every day sky monitoring.

We performed a maximum likelihood analysis at positions corresponding to every fifth degree on the map. The spacing was chosen to ensure that the analyses would be independent from one another. The position is kept fixed and the flux allowed to vary, implying one additional parameter in the alternative hypothesis. We repeated the counts map simulations and analysis for different values of the coefficient of the isotropic diffuse component ( $g_{iso}=6$  and  $12$ ) consistent with values found in real AGILE observations. Figure 2 shows the resulting  $T_s$  distribution (left panel) and the related  $p$ -value distribution (right panel). We fit this  $T_s$  distribution with the following function:

$$\kappa'(T_s) = \begin{cases} \delta & \text{if } T_s < 1 \\ \eta \chi_N^2(T_s) & \text{otherwise} \end{cases} \quad (3)$$

In Table 2 we report the results of the fit for different background  $g_{iso}$  levels. The function  $\delta$  in the first bin takes into account the constraint on the source counts ( $s_c \geq 0$ ). In this simple case, the simulated distribution is close to the expected  $1/2\chi_1^2$  (see the  $\eta$  parameter in Table 2).

In Table 3 we report the results of the fit for different levels of exposure. Figure 1 shows the regions with different exposure levels.

**Table 2.** Best fit parameters in the case of an empty field for simulated sky maps with bin size of  $0^\circ.25$  for different values of  $g_{iso}$ , the isotropic emission coefficient. The fitting function is reported in Equation 3.

$g_{iso}$	$\delta$	$\eta$
6	$0.8742 \pm 1.9 \cdot 10^{-4}$	$0.4082 \pm 2.3 \cdot 10^{-4}$
12	$0.8681 \pm 1.5 \cdot 10^{-4}$	$0.4280 \pm 2.0 \cdot 10^{-4}$

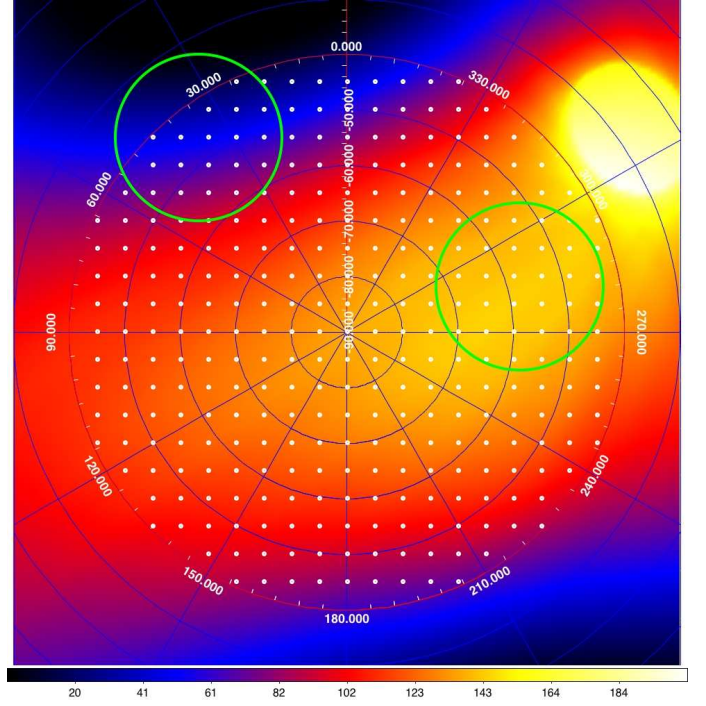


**Fig. 1.** Extra-Galactic ( $b = 90^\circ$ ) exposure map used for the simulations (in units of  $cm^2 ssr$ ) in Galactic coordinates. Notice the larger exposure near the celestial pole. The white circles are the positions of the trials, the green circles indicate the high and low chosen exposure regions.

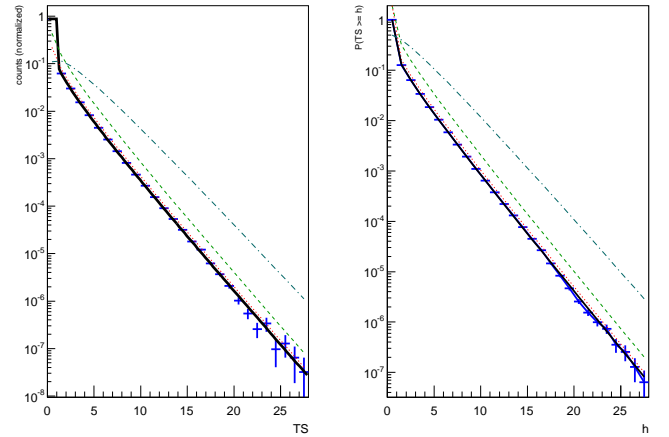


**Fig. 2.**  $T_s$  distribution (left side) and  $p$ -distribution (right side) of a simulated empty field, with  $g_{gal} = 1$  and  $g_{iso} = 6$  (with these parameters left free during the analysis), flux free, position fixed. The blue crosses are the calculated distribution, the black line is the best fit according to Equation 3, the red dotted line is the  $\frac{1}{2}\chi_1^2$  theoretical distribution, the green dashed line is the  $\frac{1}{2}\chi_2^2$  theoretical distribution, the Cyan dotted-dashed line is the  $\frac{1}{2}\chi_3^2$  distribution.

### 4.2. Real observation

We compared the simulated data shown in the last section to a real AGILE observation. The observation block chosen is OB7410 (see ASI Data Center web site, <http://agile.asdc.asi.it/>), in which AGILE was pointed to the North Galactic Pole with

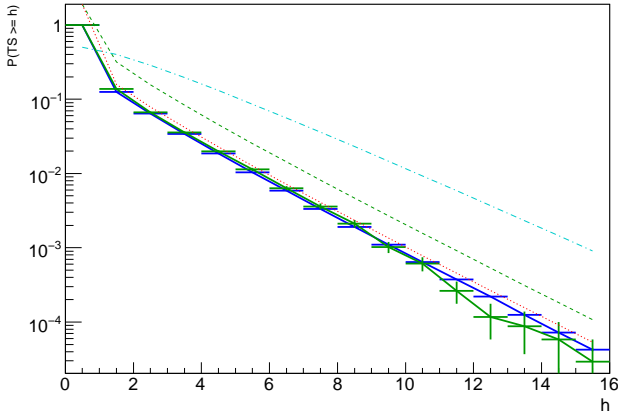
**Table 1.** Parameters and number of trials for the performed extra-Galactic and Galactic field simulations.

simulation	source position	$t_{icl}$	Simulated ( $g_{gal}, g_{iso}$ )	Analyzed $g_{gal}$ and $g_{iso}$	Trials $\times 10^6$
Extra-Gal. empty field	fixed	na	(1.0, 6.0)	free	31.0
Extra-Gal. empty field	fixed	na	(1.0, 12.0)	free	35.0
Gal. field without sources	fixed	na	(1.0, 6.0)	free	7.0
Gal. field without sources	free	5.99147	(1.0, 6.0)	fixed	4.0
Gal. field with steady sources	fixed	na	(0.63, 7.70)	fixed	9.0
Gal. field with steady sources	free	5.99147	(0.63, 7.70)	fixed	17.0
Gal. field with steady sources	free	2.29575	(0.63, 7.70)	fixed	2.2

**Table 3.** Best fit parameters in the case of an empty field for simulated sky maps with bin size of  $0^\circ.25$ ,  $g_{iso}=6$ , for two levels of exposure. The fitting function is reported in Equation 3.

exposure	$\delta$	$\eta$
low	$0.8792 \pm 5.6 \cdot 10^{-4}$	$0.3920 \pm 6.7 \cdot 10^{-4}$
high	$0.8715 \pm 5.3 \cdot 10^{-4}$	$0.4172 \pm 6.6 \cdot 10^{-4}$

good exposure. For each day of the observation counts, exposure and gas maps were generated and analyzed. As in the Monte Carlo simulations, a maximum likelihood analysis was performed for a hypothetical source position at every fifth degree to ensure the independence of each trial. The results are shown in Figure 3. Taking into account the limits of the statistics collected from this real observation, real and simulated data are compatible at  $1\sigma$  error level.


**Fig. 3.** Comparison between  $p$ -value distributions for simulated (blue) and real (green) empty extra-Galactic fields. The red dotted line is the  $\frac{1}{2}\chi_1^2$  theoretical distribution, the green dashed line is the  $\chi_2^2$  theoretical distribution, the Cyan dotted-dashed line is the  $\frac{1}{2}\chi_3^2$  distribution.

## 5. Monte Carlo simulations of Galactic fields

We performed simulations of two regions of the Galactic plane: a Galactic region with a low density of potential sources, and a complex Galactic region (the Cygnus region). These two regions represent two extremes for the AGILE analysis.

### 5.1. A simple Galactic region

We performed a simulation of a relatively simple Galactic region by assuming only the Galactic diffuse and isotropic emissions without steady or flaring sources. This calculation was aimed at evaluating the photon density function and the  $p$ -value distribution of the AGILE likelihood maximum estimator in the presence of the Galactic diffuse emission. We chose a region centered on (l,b)=(160,0) (Galactic coordinates) with 1-day exposure level in pointing mode. The parameters used in the simulation are  $g_{gal} = 1$  and  $g_{iso} = 3$ . During the analysis, the spectrum of any hypothetical source is kept fixed.

In order to analyze the flux of a source whose position is known, we fix the position of the source, and allow the flux to vary in the alternative hypothesis. The resulting  $p$ -value distribution is shown as the brown histogram in Figure 4. Using Equation 3 we find the best fit with  $\delta = 0.8600 \pm 0.0003$  and  $\eta = 0.4540 \pm 0.0005$ , for  $N_1 = 1$ . However, because of the presence of systematic errors in the event reconstruction, there are cases in which the source is detectable but at a position farther from the known position than a purely statistical analysis would predict. In order to handle these cases, we kept the position of the source free and we have developed an analysis criterion which we call ICL (Inside Confidence Contour Level): if the contour level is present,  $T_s \geq t_{ICL}$  (we fix  $t_{ICL} = 9$  for the AGILE analysis), and the position of the source under investigation is outside the contour level found by the maximum likelihood procedure, we reset  $T_s$  to 0; a contour in principle always exists (even if it is not necessarily closed or connected), but sometimes our software fails to find it. The contour is always searched for at  $t_{icl}$ .

We use the ICL criterion only in the case of the presence of a known source. The  $T_s$  distribution presented hereafter with position free and without ICL criterion are related to the analysis of an unknown source. The reason for throwing out the event is that the technique is used to weed out detections which we are not sure are coincident with the source.

We compare the results with the ICL criterion with the standard analysis (position left free). The  $p$ -value distributions are reported in Figure 4 (the red histogram for the ICL criterion, the blue histogram without the ICL criterion, both with  $T_{ss} = 4$ ,  $t_{icl} = 5.99147$ ). The blue and red histograms show a pronounced dip just above  $T_{icl}$  with respect to the brown histogram because sources with  $T_s > T_{icl}$  may increase their  $T_s$  during relocalization (shift to the right). We characterize the  $T_s$  distribution produced by the addition of the ICL criterion because it is used by the AGILE automated quick-look analysis when searching for flares from known sources.

Figure 5 reports the  $T_s$  distribution when the null hypothesis is true produced by maximum likelihood analysis with the following parameters:  $T_{ss} = 4$ ,  $t_{icl} = 5.99147$ , flux and posi-

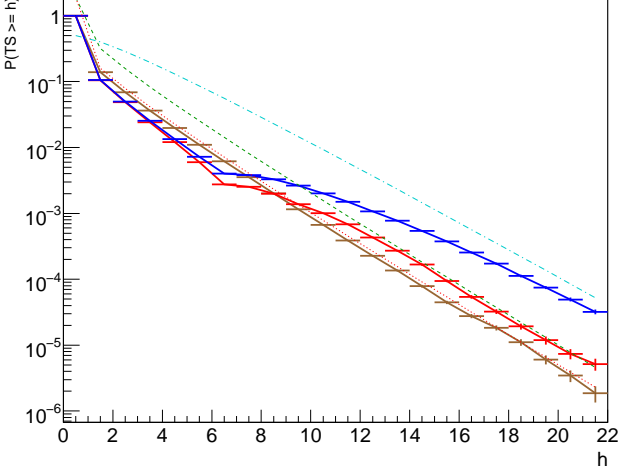


**Fig. 4.** The effect of the hypothesis formulation (trial selection). The  $p$ -value distribution depends on the constraint on the position of the source: comparison between different analysis methods (in particular, keeping fixed and leaving free the position of the source) in the case of absence of a source at the  $(l,b)=(160,0)^\circ$  location. Histograms are the  $p$ -value distribution for an empty Galactic field when the null hypothesis is true. Blue and red histograms have the following parameters:  $T_{ss} = 4$ ,  $t_{icl} = 5.99147$ , flux and position of the source left free. The blue histogram contains all trials regardless of the calculated position, while the red histogram contains the trials that respect the ICL criterion. The brown histogram has the position of the source kept fixed and flux free. The red dotted line is the  $\frac{1}{2}\chi_1^2$  theoretical distribution, the green dashed line is the  $\chi_1^2$  theoretical distribution, the cyan dotted-dashed line is the  $\frac{1}{2}\chi_3^2$  distribution.

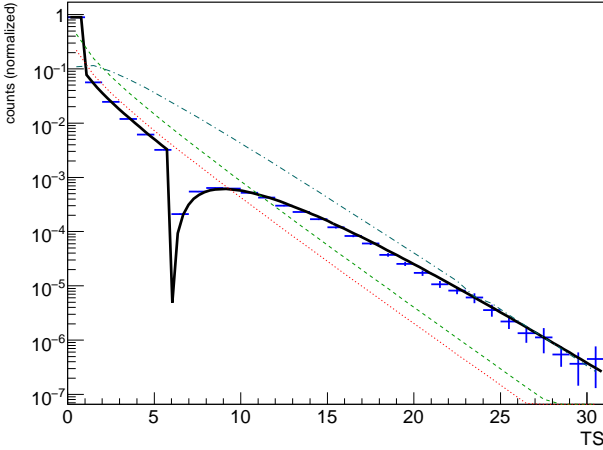


**Fig. 5.** The blue histogram is the  $T_s$  distribution for the empty Galactic region when the null hypothesis for a source at the position  $(l,b)=(160,0)^\circ$  is true.  $T_{ss} = 4$ ,  $t_{icl} = 5.99147$ , flux and position of the source left free. Black line is the best fit function described in Equation 4,  $N_2 = 5$ . The red dotted line is the  $\frac{1}{2}\chi_1^2$  theoretical distribution, the green dashed line is the  $\chi_1^2$  theoretical distribution, the cyan dotted-dashed line is the  $\frac{1}{2}\chi_3^2$  distribution.

tion of a source at  $(l,b)=(160,0)^\circ$  position left free. The related  $p$ -value distribution has been already shown in Figure 4 (blue histogram). The ICL criterion is not applied, i.e. no rejection is applied on the basis of the compatibility of the location contour with the position of the source. Fitting this distribution with the following function,

$$\kappa''(T_s) = \begin{cases} \delta & \text{if } T_s < 1 \\ \eta_1 \chi_{N_1}^2(T_s) & \text{if } T_s \geq 1 \text{ and } T_s \leq t_{icl} \\ \eta_2 \chi_{N_2}^2(T_s - t_{icl}) & \text{otherwise} \end{cases} \quad (4)$$

we find  $N_1 = 1$  (if  $T_s < T_{ss}$ , no optimization of the position takes place and therefore the only free parameter is the flux of the source),  $N_2 = 5$ ,  $\delta = 0.89 \pm 4.5 \times 10^{-4}$ ,  $\eta_1 = 0.35 \pm 5.1 \times 10^{-4}$  and  $\eta_2 = 3.96 \times 10^{-3} \pm 3 \times 10^{-5}$ . We use functions with  $N=5$  (dof) solely as an analytical approximation to the functional form produced by this process. The translation  $(T_s - t_{icl})$  is due to the switch between the fixed and free position regime (see Sect. 2).

Equation 4 is appropriate for blind searches for unknown sources. When searching for flares from a known source (i.e. our hypothesis is that there is a known source at  $(l,b)=(160,0)^\circ$  position), the appropriate alternative hypothesis should exclude sources for which the known source position lies outside the location contour. Therefore, applying the ICL rejection criterion at the 95% confidence level, the resulting  $p$ -value distribution is reported in Figure 4 (red line) compared with the blue histogram of the same Figure in which no selection criterion is applied. The effect of appropriate hypothesis formulation is evident. The application of the ICL rejection reduces the number of degrees of freedom. When we fit this distribution with Equation 4 we find that the histogram has a distribution between  $N_2 = 3$  and  $N_2 = 4$ , due to the ICL selection criterion.

The following is the analytical expression that can be used with  $t_{ICL} = 9$  where  $T_3 = 14$ :

$$\kappa'''(T_s) = \begin{cases} \delta & \text{if } T_s < 1 \\ \eta_1 \chi_{N_1}^2(T_s) & \text{if } T_s \geq 1 \text{ and } T_s \leq t_{icl} \\ \eta_2 \chi_{N_2}^2(T_s - t_{icl}) & \text{if } T_s \geq t_{icl} \text{ and } T_s \leq T_{ICL} \\ \eta_3 \chi_{N_3}^2(T_s) & \text{if } T_s \geq T_{ICL} \text{ and } T_s \leq T_3 \\ \eta_4 \chi_{N_4}^2(T_s) & \text{if } T_s \geq T_3 \end{cases} \quad (5)$$

for the following values for the parameters:  $N_1 = 1$ ,  $N_2 = 5$ ,  $N_3 = 5$ ,  $N_4 = 1$ ,  $\delta = 0.89 \pm 4.4 \times 10^{-4}$ ,  $\eta_1 = 0.34 \pm 5.1 \times 10^{-4}$ ,  $\eta_2 = 4.5 \times 10^{-3} \pm 5.7 \times 10^{-5}$ ,  $\eta_3 = 1.27 \times 10^{-2} \pm 1.7 \times 10^{-4}$ ,  $\eta_4 = 0.91 \pm 3.3 \times 10^{-2}$ . This expression approximates the expected behavior of the analysis, which shifts gradually from a source location algorithm with many free parameters near the threshold where the location contour is large, to an analysis more similar to a fixed-position analysis at high  $T_s$  where the location contour is small. Figure 6 reports the  $T_s$  distribution when the null hypothesis is true produced by maximum likelihood analysis with the following parameters:  $T_{ss} = 4$ ,  $t_{icl} = 5.99147$ , flux and position left free and ICL criterion; red histogram is of a region centered at  $(l,b)=(160,0)^\circ$ , blue histogram is related to Cygnus region. The black line is the best fit as reported in Eqn. 5. The reported distributions correspond to the standard quick-look analysis of AGILE data for empty Galactic regions. We notice that the changes in the selection criterion modify the expected  $p$ -values with respect to the  $\frac{1}{2}\chi_3^2$  theoretical expected distribution (cyan dashed line).

The analysis with the position of the source kept fixed yields lower  $p$ -values than the analysis with the position allowed to vary, either with the ICL criterion (red histogram of Figure 4)

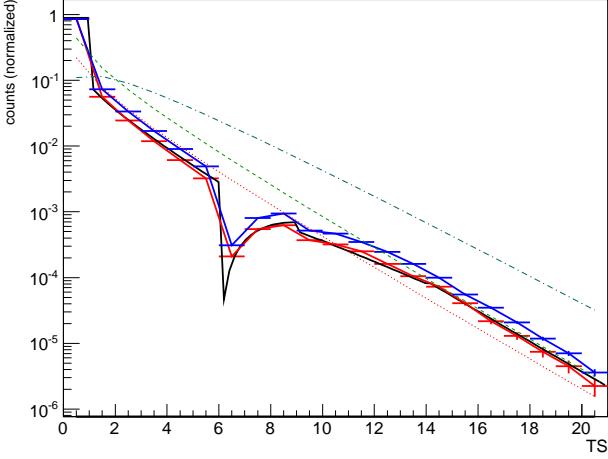


**Fig. 6.** The effect of steady sources in the ensemble of models. The blue line is the PDF for Cygnus field when the null hypothesis for Cygnus X-3 is true, and the red line is the PDF for an empty Galactic field when the null hypothesis is true, with the following parameters:  $T_{ss} = 4$ ,  $t_{icl} = 5.99147$ , flux and position of source in the alternative hypothesis left free,  $g_{gal}$  and  $g_{iso}$  parameters fixed, ICL criterion. Black line is the best fit function described in Equation 5. The red dotted line is the  $\frac{1}{2}\chi^2_1$  theoretical distribution, the green dashed line is the  $\chi^2_1$  theoretical distribution, the Cyan dotted-dashed line is the  $\frac{1}{2}\chi^2_3$  distribution.

or without (blue histogram). However, the fraction of detections above a given  $T_s$  threshold in the presence of a real source is also lower when the source position is kept fixed, as shown by the histograms in Figure 7. Table 4 reports the number of detections (in %) for some  $T_s$  thresholds.

### 5.2. A complex Galactic region: the case of the Cygnus field

We simulated observations of the Cygnus region both including and without a source at the position of Cygnus X-3 to test the analysis procedure in a complex case with nearby point sources and Galactic diffuse emission. We have chosen this field because this is one of the most complex cases that our analysis procedure must address. Cygnus X-3 is a well-known microquasar (Giacconi et al. 1967), showing variable emission at all wavelengths, including repeated  $\gamma$ -ray flaring activity above 100 MeV as detected by AGILE (Tavani et al. 2009b). This case has been chosen because it shows a great variability in the  $\gamma$ -ray energy range and a high correlation with other wavelengths. The list of simulated sources of the Cygnus region is reported in Table 5. In Figure 8 we show a 0.5 year integration of AGILE data from the Cygnus region and a simulation of a comparable integration using the same parameters used to simulate the short trials, demonstrating that the underlying model is sound.

The null hypothesis is that no  $\gamma$ -ray source coincident with Cygnus X-3 is present in the AGILE data, while the alternative hypothesis is that a source coincident with Cygnus X-3 is emitting  $\gamma$ -rays. The parameters of the other sources and the diffuse emission coefficients were all kept fixed.

If we fix the position of the source as already described in the previous section, using Equation 3 we find the best fit with  $\delta = 0.65 \pm 3.6 \times 10^{-4}$ ,  $\eta = 4.6 \times 10^{-1} \pm 4.2 \times 10^{-4}$ ,  $N_1 = 1$ . The two  $\eta$  parameters of the cases of empty and complex Galactic fields

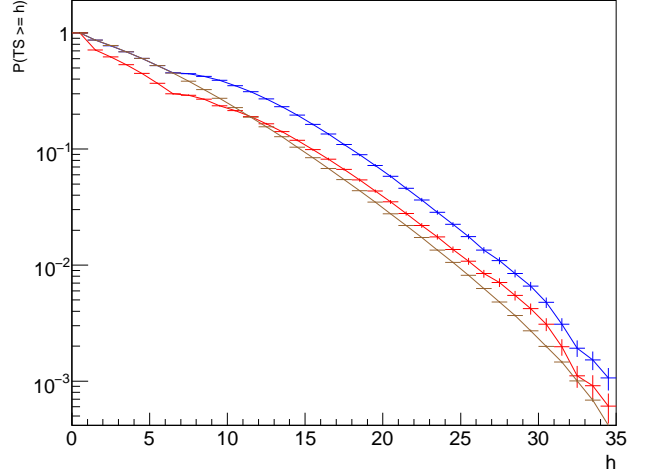


**Fig. 7.** The effect of the hypothesis formulation (trial selection). The histograms show the  $p$ -value distributions in the presence of a simulated source at the location of  $(l,b)=(160,0)^\circ$  with flux  $180 \times 10^{-8}$  photons  $\text{cm}^{-2} \text{s}^{-1}$ . Red histograms have the following parameters:  $T_{ss} = 4$ ,  $t_{icl} = 5.99147$ , flux and position of the source left free with ICL rejection criterion. Blue histograms have  $t_{icl} = 5.99147$ , flux and position of the source left free without ICL rejection criterion. Brown histograms have the flux left free and the position of the source kept fixed.

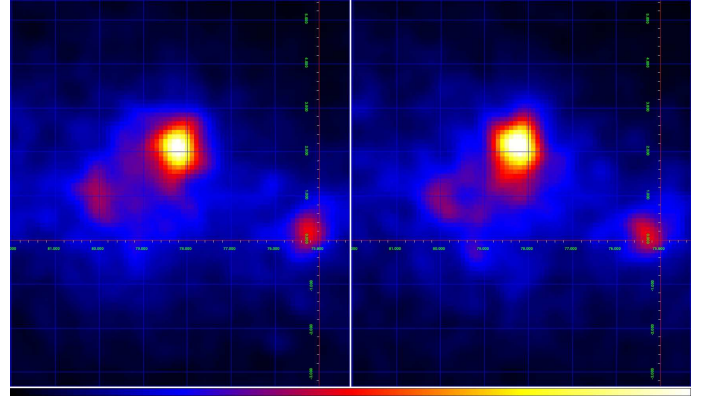


**Fig. 8.** The binned counts map of the real (left side) and simulated (right side) Cygnus field for an integration time of 0.5 years (AGILE counts,  $E > 100$  MeV). The real data is taken from July 2007 to October 2009; the map is centered on  $(l,b)=(78.75, 0)^\circ$  in Galactic coordinates with a bin size of  $0.1^\circ$ .

are very similar. Therefore, in the Tables 6 and 8 we report a single value for the fixed position analysis which is valid for both cases.

Keeping the position of Cygnus X-3 free and fitting with Equation 4 we find that  $N_1 = 1$ ,  $N_2 = 5$ ,  $\delta = 0.85 \pm 4.6 \times 10^{-4}$ ,  $\eta_1 = 0.46 \pm 6.2 \times 10^{-5}$  and  $\eta_2 = 6.15 \times 10^{-3} \pm 0.4 \times 10^{-5}$ . This fitting is appropriate for blind searches for unknown sources in complex Galactic regions.

Keeping the position of Cygnus X-3 free with ICL criterion and fitting with Equation 5 we find that  $N_1 = 1$ ,  $N_2 = 5$ ,  $N_3 = 5$ ,  $N_4 = 1$ ,  $\delta = 0.84 \pm 2 \times 10^{-4}$ ,  $\eta_1 = 0.49 \pm 2.8 \times 10^{-4}$ ,  $\eta_2 = 6.7 \times 10^{-3} \pm 3.2 \times 10^{-5}$ ,  $\eta_3 = 1.8 \times 10^{-2} \pm 1.0 \times 10^{-5}$ ,  $\eta_4 = 1.32 \pm 1.9 \times 10^{-2}$ . This expression approximates the expected behavior of the analysis, as already established in the case of an

**Table 4.** % of detections for some  $T_s$  thresholds (with related  $p$ -values when the null hypothesis is true) when the null hypothesis is false with a source at the  $(l,b)=(160,0)^\circ$  position with a simulated flux of  $180 \times 10^{-8}$  photons  $\text{cm}^{-2} \text{s}^{-1}$ .

$T_s \geq$	Fixed position		Free position 95%		Free position 95% + ICL	
	% detection	$p$ -value	% detection	$p$ -value	% detection	$p$ -value
12	18.1	$2.48 \times 10^{-4}$	31.3	$1.21 \times 10^{-3}$	22.3	$4.44 \times 10^{-4}$
16	6.2	$2.95 \times 10^{-5}$	16.1	$2.98 \times 10^{-4}$	10.4	$5.81 \times 10^{-5}$
25	0.7	$2.68 \times 10^{-7}$	2.2	$7.61 \times 10^{-6}$	1.3	$5.26 \times 10^{-7}$

Fixed position: source position fixed, flux free,  $T_{ss} = 4$ ,  $g_{gal}$  and  $g_{iso}$  parameters fixed.

Free position 95%: source position free, flux free,  $t_{lcl} = 5.99147$ ,  $T_{ss} = 4$ ,  $g_{gal}$  and  $g_{iso}$  parameters fixed.

Free position 95% + ICL: source position free, flux free,  $t_{lcl} = 5.99147$ ,  $T_{ss} = 4$ ,  $g_{gal}$  and  $g_{iso}$  parameters fixed, ICL rejection.

**Table 5.** List of Cygnus region sources for  $E > 100$  MeV.

AGILE Name	l	b	E>100 MeV			Counterpart name
			$\sqrt{TS}$	Flux		
AGL 2021+4029	78.24	2.16	42.1	$141 \pm 4$		Gamma Cygni
AGL 2021+3652	75.24	0.14	23.3	$67 \pm 3$		PSR J2021+3651
AGL 2030+4129	80.11	1.25	8.1	$18 \pm 3$		LAT PSR J2032+4127
AGL 2026+3346	73.28	-2.49	6.8	$10 \pm 1.7$	-	
AGL 2046+5032	88.99	4.54	6.5	$10 \pm 1.7$	-	
AGL 2016+3644	74.59	0.83	6.3	$14 \pm 2.3$	-	
AGL 2029+4403	81.97	3.04	5.4	$14 \pm 3$	-	
AGL 2038+4313	82.32	1.18	5.1	$15 \pm 3$	-	
AGL 2024+4027	78.56	1.63	5.0	$24 \pm 5$	-	
AGL 2019+3816	76.24	1.14	4.2	$11 \pm 2.4$	-	
AGL 2036+3954	79.47	-0.56	3.4	$5.0 \pm 1.5$	-	

The table provides: (1) AGILE name of the sources; (2) (3) the galactic coordinates  $l$  and  $b$ ; (4) the statistical significance  $\sqrt{TS}$  of the source detection according to the maximum likelihood ratio test for  $E > 100$  MeV; (5) the period-averaged flux  $F$  ( $E > 100$  MeV) in  $10^{-8}$  photons  $\text{cm}^{-2} \text{s}^{-1}$  for  $E > 100$  MeV; (6) a possible counterpart. We added more sources in the  $\gamma$ -ray model compared with the First AGILE Catalog (Pittori et al. 2009) to take into account a new background event filter (FM3.119).

empty Galactic field (see Section 5.1). The reported distributions correspond to the standard quick-look analysis of AGILE data for complex Galactic regions.

Figure 6 compares the probability density function for the Cygnus field (see Table 5) with this empty Galactic field. As expected, the effect of a more complex region is an increase in the number of false detections.

With the performed Monte Carlo simulation we have determined the  $p$ -value function for the most common hypothesis formulations. Based on these simulation we are able to establish the  $T_s$  level for each  $p$ -value and constrain the false occurrence rate. Table 6 reports the correspondence between  $p$ -value and  $T_s$  value for different methods of analysis, in addition to the theoretical reference for  $\chi_1^2$ ,  $1/2\chi_1^2$  and  $1/2\chi_3^2$ .

### 5.3. Deviation from the nominal distribution

In the following we report the effect that uncertainties in the analysis parameters produce on the shape of the distributions. The analyses were performed for the case of the complex Galactic region.

#### 5.3.1. The effect of the $t_{lcl}$ parameter

We performed additional maximum likelihood analyses using different values of the  $t_{lcl}$  parameter, including the case of  $t_{lcl} = 0$ . In the case of a blind search for unknown sources, the maxi-

mum likelihood estimator can be used as a source finder, instead of an hypothesis validator, by setting  $t_{lcl} = 0$ . In this case the optimization of the position is performed regardless of the  $T_s$  found in the first step with fixed position. The resulting  $p$ -value distributions are shown in Figure 9 (with  $t_{lcl} = 0$  shown in green) including all trials without ICL rejection. As expected, higher  $t_{lcl}$  values correspond to lower  $p$ -values because the optimization of the position starts for higher  $T_s$  values in the first loop of the maximum likelihood procedure.

#### 5.3.2. The effect of the radius of analysis

Figure 10 shows that no appreciable differences are produced by changing the radius of analysis. The comparison was performed for the case of  $t_{lcl} = 0$  applying the ICL criterion, but should also be valid for analyses using the other criteria.

#### 5.3.3. The effect of of keeping $g_{gal}$ and $g_{iso}$ free or fixed

In Figure 11 we show the effect of keeping  $g_{gal}$  and  $g_{iso}$  parameters fixed (blue) and free (red): the  $p$ -values with free parameters are larger. This result is expected because fixing these parameters reduces the range of possible hypotheses explored. The comparison was performed for the case of  $t_{lcl} = 0$  applying the ICL criterion, but should also be valid for analyses using the other criteria.



**Table 6.** Correspondence between  $p$ -value and  $T_s$  value for different methods of analysis. The first column reports the  $p$ -value, the following columns report the corresponding  $T_s$  value. In particular, the fifth column reports the corresponding  $T_s$  value for Galactic regions with the position of the source of the alternative hypothesis kept fixed, the sixth and last columns report the corresponding  $T_s$  value for Galactic regions (first number for empty regions, second number for complex regions) with the position of the source of the alternative hypothesis kept free.

$p$ -value	$\chi_1^2$	$1/2\chi_1^2$	$1/2\chi_3^2$	$T_s$		
				Fixed position	Free position 95%	Free position 95% + ICL
$10^{-2}$	6.63	5.41	9.84	5.29	4.78-5.27	4.78-5.41
$10^{-3}$	10.83	9.55	14.80	9.42	12.60-13.90	9.89-10.84
$10^{-4}$	15.14	13.83	19.66	13.70	18.81-19.91	14.97-15.67
$10^{-5}$	19.52	18.19	24.47	18.06	24.36-25.40	19.35-20.05
$10^{-6}$	23.93	22.60	29.23	22.46	29.66-30.66	23.76-24.47
$10^{-7}$	28.37	27.03	33.98	26.90	34.81-35.79	28.21-28.92
$10^{-8}$	32.83	31.49	38.71	31.36	39.87-40.84	32.67-33.39
$10^{-9}$	37.32	35.97	43.42	35.84	44.87-45.82	37.16-37.87

Fixed position: source position fixed, flux free,  $T_{ss} = 4$ ,  $g_{gal}$  and  $g_{iso}$  parameters fixed.

Free position 95%: source position free, flux free,  $t_{lcl} = 5.99147$ ,  $T_{ss} = 4$ ,  $g_{gal}$  and  $g_{iso}$  parameters fixed.

Free position 95% + ICL: source position free, flux free,  $t_{lcl} = 5.99147$ ,  $T_{ss} = 4$ ,  $g_{gal}$  and  $g_{iso}$  parameters fixed, ICL rejection.

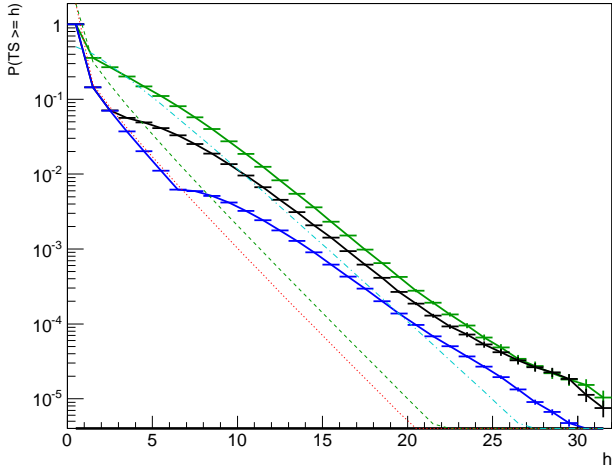


**Fig. 9.** The  $p$ -value distributions change as a function of the  $t_{lcl}$  parameter. Simulations of the Cygnus region with no source present at Cygnus X-3 position were analyzed with different  $t_{lcl}$  values without applying the ICL rejection criterion. The flux and position of the hypothetical source at the Cygnus X-3 were allowed to vary, the  $g_{gal}$  and  $g_{iso}$  parameters were kept fixed, and  $T_{ss} = 4$ . Green histogram:  $t_{lcl} = 0$ ; black histogram:  $t_{lcl} = 2.29575$  (corresponds to a 68% confidence level for two degrees of freedom); blue histogram:  $t_{lcl} = 5.99147$ . The red dotted line is the  $\frac{1}{2}\chi_1^2$  theoretical distribution, the green dashed line is the  $\chi_1^2$  theoretical distribution, and the cyan dotted-dashed line is  $\frac{1}{2}\chi_3^2$  distribution.

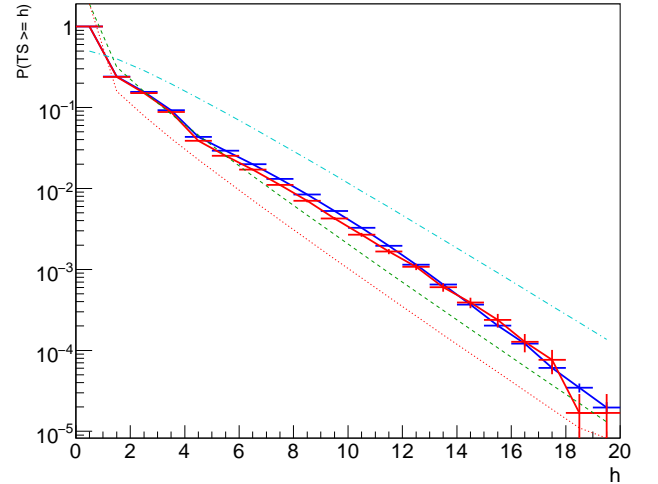


**Fig. 10.** Comparison between different radii of analysis. The histograms are the  $p$ -value distributions for the Cygnus field when the null hypothesis for Cygnus X-3 is true with the following parameters:  $T_{ss} = 4$ ,  $t_{lcl} = 0$ , flux and position of Cygnus X-3 left free, ICL rejection applied. Red histogram: radius of analysis =  $10^\circ$ ; blue histogram: radius of analysis =  $5^\circ$ . The red dotted line is the  $\frac{1}{2}\chi_1^2$  theoretical distribution, the green dashed line is the  $\chi_1^2$  theoretical distribution, and the cyan dotted-dashed line is the  $\frac{1}{2}\chi_3^2$  distribution.

### 5.3.4. The effect of unmodeled point sources

We performed a Monte Carlo simulation in which the simulated data contain all of the sources listed in Table 5, followed by a maximum likelihood analysis with models containing only a point source at the location of Cygnus X-3, in order to evaluate the effect of nearby unmodeled point sources. The resulting  $p$ -value distribution is shown in Figure 12, where the red histogram

is the  $p$ -value distribution with the analysis models containing all the sources used in the simulation and the black histogram is the  $p$ -distribution with only the source at the Cygnus X-3 location. This illustrates that it is critical to model existing sources correctly.

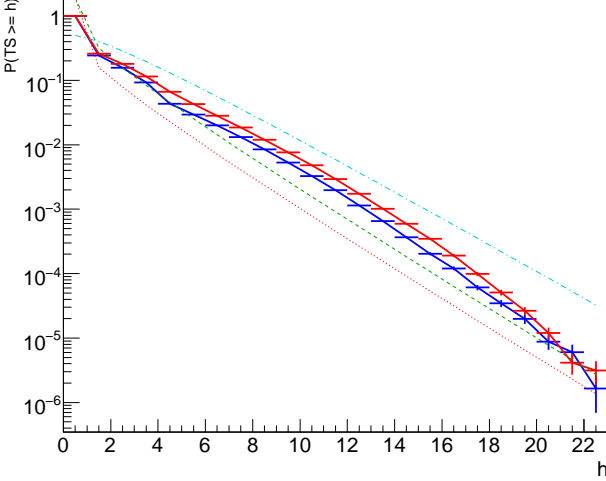


**Fig. 11.** Comparison between  $g_{gal}$  and  $g_{iso}$  parameters free or fixed. The blue histogram is the  $p$ -distribution for the Cygnus field when the null hypothesis for Cygnus X-3 is true with the following parameters:  $T_{ss} = 4$ ,  $t_{lcl} = 0$ , flux and position of Cygnus X-3 left free,  $g_{gal}$  and  $g_{iso}$  parameters fixed. The red histogram has the same parameters but with  $g_{gal}$  and  $g_{iso}$  parameters left free. The red dotted line is the  $\frac{1}{2}\chi_1^2$  theoretical distribution, the green dashed line is the  $\chi_1^2$  theoretical distribution, the cyan dotted-dashed line is the  $\frac{1}{2}\chi_3^2$  distribution.

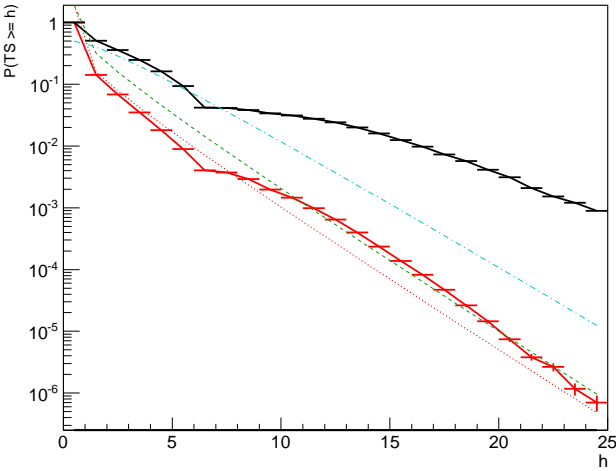


**Fig. 12.** The effect of unmodeled sources. The histograms are the  $p$ -value distribution for the Cygnus field when the null hypothesis for Cygnus X-3 is true with the following parameters:  $T_{ss} = 4$ ,  $t_{lcl} = 5.99147$ , flux and position of Cygnus X-3 left free,  $g_{gal}$  and  $g_{iso}$  parameters fixed. The red histogram shows the result when all the simulated sources are included in the models, while the black histogram shows the result when only the source at Cygnus X-3 position is included. The red dotted line is the  $\frac{1}{2}\chi_1^2$  theoretical distribution, the green dashed line is the  $\chi_1^2$  theoretical distribution, the cyan dotted-dashed line is the  $\frac{1}{2}\chi_3^2$  distribution.

### 5.3.5. The effect of errors in the diffuse emission: estimating using $g_{gal}$

We performed a preliminary investigation of the effect of systematic errors in the diffuse emission model on the analysis results by fixing the  $g_{gal}$  parameter during the analysis at a value  $g_{gal} = 0.67$  different from the one used in simulating the data;  $g_{iso} = 7.7$  is simulated but the  $g_{iso}$  parameter is left free to adapt during the analysis. Figure 13 reports the  $p$ -value distributions for the Cygnus field when the null hypothesis for Cygnus X-3 is true where the results of three analyses are compared; one with simulated  $g_{gal} = 0.67$  (blue thick lines), one with simulated  $g_{gal} = 0.67 * 1.1$  (red thick lines) and one with simulated  $g_{gal} = 0.67 * 0.89$  (black thick lines). Table 7 reports the resulting calculated  $g_{iso}$ .

**Table 7.** The mean value of the calculated  $g_{iso}$  parameter

Simulations		Analysis	
$g_{gal}$	$g_{iso}$	$g_{gal}$ fixed	$g_{iso}$ calculated
$0.67 * 0.89$	7.7	0.67	$6.55 \pm 1.46$
0.67	7.7	0.67	$7.55 \pm 1.52$
$0.67 * 1.1$	7.7	0.67	$8.52 \pm 1.59$

As expected,  $g_{iso}$  moves up if  $g_{gal}$  is too small and vice versa. If  $g_{gal}$  is under-estimated, then the number of false detections when the source is absent increases (see the red lines of Figure 13), because background photons are assigned to the source. If the  $g_{gal}$  parameter is over-estimated, then the number of false detections when the source is absent decrease (see black line of Figure 13) because the diffuse model is already too high at the position of Cygnus X-3.

## 6. Pre-trials and post-trials significance

We have seen how the Monte Carlo simulations can be used to characterize the  $T_s$  distributions produced by the AGILE-GRID maximum likelihood analysis procedure. In the end, we find the probability, or  $p$ -value, of finding a false positive detection (rejecting the null hypothesis when it is true) in a single observation.

In practice, for each region of the sky we perform many trials during the daily monitoring to search for transient  $\gamma$ -ray events. The probability of obtaining a single false detection over a large number of trials is therefore much higher than  $p$ . In the AGILE context we perform two kinds of analysis for each analyzed map:

1. blind search for unknown sources: we search for more than one source at a time with free positions;
2. searches from a list of known sources: we search for more than one source at a time with fixed source positions.

Let  $K = M \cdot N$  the number of independent trials, where  $N$  is the number of maps and  $M$  is the number of unknown sources in the first case or the number of sources in the predefined list in the second case. If we have only one source in both cases  $M = 1$ .

Since the probability of *not* making a false positive error in a single trial is  $1 - p$ , the probability of not making any false positive error is  $(1 - p)^K$  (type-I error), so the probability of making at least one false positive error is  $\pi = 1 - (1 - p)^K$ . This is defined as the post-trial probability, also referred to as the *experiment-wide error rate*, while  $p$  is denoted as the pre-trial probability, or

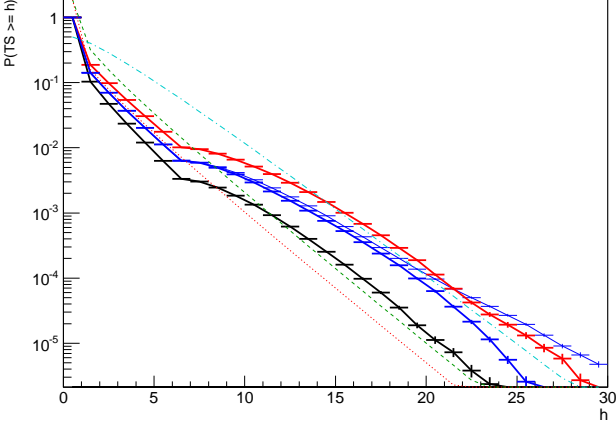


**Fig. 13.** The effect of a poor estimation of the Galactic diffuse emission. The histograms are the  $p$ -value distributions for the Cygnus field when the null hypothesis for Cygnus X-3 is true with the following parameters:  $T_{ss} = 4$ ,  $t_{icl} = 5.99147$ , flux and position of Cygnus X-3 left free. The true value of  $g_{iso}$  in the simulated data is 7.7, the value of  $g_{gal}$  used in the analysis is fixed to 0.67. Blue thin line: simulated  $g_{gal} = 0.67$ ,  $g_{iso}$  fixed to 7.7; blue thick line: simulated  $g_{gal} = 0.67$ ,  $g_{iso}$  left free; red thick line: simulated  $g_{gal} = 0.67 * 1.1$ ,  $g_{iso}$  left free; black thick line: simulated  $g_{gal} = 0.67 * 0.89$ ,  $g_{iso}$  left free. The red dotted line is the  $\frac{1}{2}\chi^2_1$  theoretical distribution, the green dashed line is the  $\chi^2_1$  theoretical distribution, the cyan dotted-dashed line is the  $\frac{1}{2}\chi^2_3$  distribution.

comparison-wise error rate. For an experiment-wide false positive rate of  $\pi$ , we can constrain the comparison-wise error rate with the Dune-Šidák correction  $p \leq 1 - (1 - \pi)^{1/K}$ .

Let us consider a typical AGILE case in the context of Galactic  $\gamma$ -ray transients with the position of the source left free and with a single source with flux and position free for each map ( $M = 1$ ): usually we keep fixed the position and flux of known sources assuming that only one source is in a flaring state in our map (we can reduce the size of the map to accomplish this). If we search for a single flaring source once every two days ( $N = 182$  for 1 year of observations in AGILE spinning mode), if we can accept one false detection during the year  $\pi \leq 1/N$ , this implies threshold of  $T_s \approx 17.9$ . If we can accept a false detection once every 2 years, the threshold is  $T_s \approx 20.5$ .

Table 8 reports the post-trial significance expressed in Gaussian standard deviations for some values of  $K$ .

## 7. Probability of sky-position coincidence in non-overlapping time intervals

In this section we generalize the analysis performed in the previous sections to calculate the probability of two or more detections of a flaring source performed in the same sky position in different independent time intervals. Multiple detections of a source can have a low probability of being consistent with the null hypothesis even when the individual detections are at a low level of  $T_s$ . In order to assess the statistical significance of our detections, we consider the post-trial probability of flare occurrence. We distinguish two cases:

1. the case of a single flare episode originating from a specific source within a given error box (that we define as “single independent occurrence” or “single post trial occurrence”);
2. the case of repeated flaring episodes originating from a specific source with a given error box (that we call here “repeated post-trial flare occurrence”).

For each individual AGILE detection, we can calculate the post-trial significance of the *single independent occurrences*, which does not take into account the history of repeated occurrences.

We can then combine the history of the sky region and establish the probability of repeated flaring episodes from the same sky position. We calculate the post-trial significance for *repeated flare occurrences* at the source error-box position as follows.

If we perform one trial for each map ( $M = 1$ , we use a list with only one source; this means that each independent time period is a single trial), the chance probability of having  $k$  or more detections over  $N$  maps at a specific site with a  $T_s$  statistic satisfying  $T_s \geq h$  is given by  $P(N, X \geq k) = 1 - \sum_{j=0}^{k-1} \binom{N}{j} p^j (1-p)^{N-j}$  where  $p = p(h)$  is the  $p$ -value corresponding to the  $h$  value given by Equation 2,  $P(N, X = j) = \binom{N}{j} p^j (1-p)^{N-j}$  is the probability of exactly  $j$  detections in  $N$  maps and  $P(N, X < k) = \sum_{j=0}^{k-1} \binom{N}{j} p^j (1-p)^{N-j}$  is the probability of fewer than  $k$  detections at a specific position in  $N$  maps.

If we perform  $M$  trials in different positions of  $N$  maps, where  $M$  is the number of known or unknown sources in a predefined list, the chance of having  $k$  or more detections above the level  $h$  in any of the sites with a  $T_s$  statistic satisfying  $T_s \geq h$  is given by  $P_M(N, X \geq k) = 1 - \left( \sum_{j=0}^{k-1} \binom{N}{j} p^j (1-p)^{N-j} \right)^M$  where  $P_M(N, X \geq k) = 1 - P(N, X < k)^M = 1 - (1 - P(N, X \geq k))^M$ .

The choice of  $p(h)$  depends on our assumptions: if the flare comes from a known source we use Equation 5, if the flare comes from a previously unknown source we use Equation 4 (the case without ICL criterion).

Let us consider a simple case in the context of Galactic  $\gamma$ -ray transients, using the  $p$ -value function in the case of a complex Galactic region with the position of a single source left free. If we detect one flare per year at a specific position of the Galactic plane with  $T_s > 16$ , and we produce 182 maps per year (once every two days with an integration time of two days), then after the first year the global post-trial significance is  $2.16 \sigma$ , after the second year it is  $3.31 \sigma$ , and after the third year it is  $4.16 \sigma$ . Transient sources, as long as they recur, enable us to have more confidence in their detection as integration time increases.

It might seem that this approach adds a bias to the *global significance* of a detection of a flaring source, because it may happen that some flares from nearby sources can be “counted” together due to the extension of the 95% contour confidence level. In doubtful cases only a more detailed analysis can exclude this.

## 8. Conclusions

We have performed extensive Monte Carlo simulations to characterize the maximum likelihood ratio test for the AGILE-GRID instrument in the context of short timescale (1-2 days) flaring  $\gamma$ -ray sources, both in extra-Galactic and Galactic fields. In the case of Galactic fields, we have simulated both a simple (without

**Table 8.** Post-trial significance expressed in Gaussian standard deviations ( $\sigma$ ). The first column reports the pre-trial significance, the second column reports the corresponding  $p$ -value, the third column reports the corresponding  $T_s$  value for Galactic regions with the position of the source of the alternative hypothesis kept fixed, the fourth and fifth columns report the corresponding  $T_s$  value for Galactic regions (first number for empty regions, second number for complex regions) with the position of the source of the alternative hypothesis left free, the last two columns report the post-trial significance for  $K=180$  and  $K=360$  trials.

$\sigma$ pre-trial	$p$ -value	$T_s$			$\sigma$ post-trial	
		Fixed position	Free position 95%	Free position 95% + ICL	K=180	K=360
3	$1.35 \times 10^{-3}$	8.88	11.66-13.03	9.08-10.05	0.78	0.29
4	$3.17 \times 10^{-5}$	15.87	21.63-22.69	17.14-17.85	2.53	2.28
5	$2.86 \times 10^{-7}$	24.87	32.47-33.46	26.17-26.88	3.88	3.71
6	$9.21 \times 10^{-10}$	36.00	45.05-46.00	37.31-38.03	5.10	4.97

Fixed position: source position fixed, flux free,  $T_{ss} = 4$ ,  $g_{gal}$  and  $g_{iso}$  parameters fixed.

Free position 95%: source position free, flux free,  $t_{icl} = 5.99147$ ,  $T_{ss} = 4$ ,  $g_{gal}$  and  $g_{iso}$  parameters fixed.

Free position 95% + ICL: source position free, flux free,  $t_{icl} = 5.99147$ ,  $T_{ss} = 4$ ,  $g_{gal}$  and  $g_{iso}$  parameters fixed, ICL rejection.

steady sources) and a complex Galactic region. With these simulations we have calibrated both the  $T_s$  distributions (pre-trial significance) and the related false occurrence rate.

After the introduction of the post-trial significance, we calculated the post-trial probabilities for single and multiple occurrences. In particular, we calculated the probability of two or more detections of a flaring source at the same sky position in different independent time intervals. With this approach, we take into account the presence of many flaring episodes originating from the same sky region, combining its history and adding information not present in the single episode and in the post-trial evaluation. We call this “repeated post-trial flare occurrence”.

In this paper we have provided a method for converting the  $T_s$  produced by any of the various methods made available by the AGILE analysis software into a probability. This information can be used by anyone who performs analysis on GRID data through the AGILE Guest Observer Program.

## 9. Acknowledgements

The AGILE Mission is funded by the Italian Space Agency (ASI) with scientific and programmatic participation by the Italian Institute of Astrophysics (INAF) and the Italian Institute of Nuclear Physics (INFN). We acknowledge financial contribution from the agreement ASI-INAF I/009/10/0.

## References

- Bulgarelli, A., et al., 2009, ASP Conference Series, 411, 362
- Cash, W., 1979, ApJ, 228:939
- Giacconi, R., et al., 1967, ApJ, 148, L119
- Mattox, J. R., et al. 1996, ApJ, 461, 396-407
- Pittori, C., et al. 2009, A&A , 506, 1563
- Tavani, M., et al. 2009a, A&A , 502, 995
- Tavani, M., et al. 2009b, Nature, 462, 620
- Wilks, S. S., 1938, Ann. Math. Stat., 9, 60